

An analytic investigation of the scatter in the integrated X-ray properties of galaxy groups and clusters.

Michael L. Balogh¹, Arif Babul², G. Mark Voit³, Ian G. McCarthy^{2,4}, Laurence R. Jones⁵, Geraint F. Lewis⁶, Harald Ebeling⁷

¹Department of Physics, University of Waterloo, Waterloo, ON, Canada N2L 3G1, email: mbalogh@uwaterloo.ca

²Department of Physics and Astronomy, University of Victoria, Victoria, BC, Canada V8P 1A1

³Department of Physics and Astronomy, Michigan State University, East Lansing MI 48824 USA

⁴Department of Physics and Astronomy, University of Durham, Durham, UK, DH1 3LE

⁵Department of Physics and Astronomy, University of Birmingham, Birmingham, UK B15 2TT

⁶Institute of Astronomy, School of Physics, A29, University of Sydney, NSW 2006, Australia

⁷Institute for Astronomy, 2680 Woodlawn Drive, Honolulu, Hawaii 96822 USA

1 August 2018

ABSTRACT

We revisit the scaling relationships between the dark matter mass and observed X-ray luminosity and temperature of galaxy clusters and groups in the local Universe. Specifically, we compare recent observations with analytic models of the intracluster medium in which the gas entropy distribution has been shifted by a variable amount, K_o , to investigate the origin of the scatter in these scaling relations, and its influence on the luminosity and temperature functions. We find that variations in halo concentration or formation epoch (which might determine the time available for low entropy gas to cool out) are insufficient to explain the amount of scatter in the mass–luminosity relation. Instead, a range of entropy floors at a fixed halo mass, spanning approximately ~ 50 keV cm² to ~ 700 keV cm², is required to match the data. This range is likely related to the variance in heating and/or cooling efficiency from halo to halo. We demonstrate that these models are consistent with the observed temperature and luminosity functions of clusters, with a normalization of $\sigma_8 \sim 0.8$ in agreement with WMAP measurements (for $h = 0.7$ and $\Omega_m = 0.3$); in particular the scatter in the mass–luminosity relation has an important influence on the shape of the luminosity function, and must be accounted for to provide a consistent result. Finally, we present predictions for the redshift evolution of these scaling relations and luminosity/temperature functions. Comparison with recent data at $z < 0.7$ shows reasonable agreement with a model that assumes a median entropy floor of $K_o = 200$ keV cm². When observations are extended to group scales ($kT \lesssim 1$ keV), this evolution will have the potential to discriminate between an entropy floor that is independent of redshift (for example, in a preheating scenario) and one that depends on the cooling time of the halo.

Key words: galaxies: clusters — X-rays:galaxies:clusters — intergalactic medium

1 INTRODUCTION

The X-ray properties of clusters are tracers of both the gravitational potential and the thermodynamic history of the gas. Since the mass is likely dominated by collisionless dark matter, for which we have a well-developed theory (e.g. Evrard et al. 2002), we might hope to learn about the relevant baryonic physics through detailed X-ray observations. In particular, clusters obey fairly well defined scaling relations between mass and X-ray temperature (M-T) and mass and X-ray luminosity (M-L). Although the slope and

normalization of these relations relative to model predictions have been studied extensively (Edge & Stewart 1991; Markevitch 1998; Horner et al. 1999; Nevalainen et al. 2000; Arnaud et al. 2005), little attention has been paid to their intrinsic scatter (but see Rowley et al. 2004; Kay et al. 2004; Smith et al. 2005).

The presence of scatter in the M-L and M-T relations suggests intrinsic variations in the structure of clusters, which may be due either to variations in the dark matter distribution of the halos themselves, and/or in the gas prop-

erties. In particular, the scatter is likely to be driven by variations in the core properties of clusters, since the scatter is known to be significantly reduced if the central regions are excluded from the analysis (e.g. Markevitch 1998).

In the case of the dark matter component of relaxed clusters, there are indications that either (or both) the halo concentration parameter and the inner slope of the halo profile varies from cluster to cluster, perhaps due to cosmic environmental effects such as the extent of tidal torquing the dark matter experiences during collapse or the merger history of the halo (e.g. Jing 2000; Bullock et al. 2001; Wechsler et al. 2002; Zhao et al. 2003; Williams et al. 2004). The amount of substructure and dynamical state of the dark matter will also vary and depend upon the merging history of the halo.

There are also reasons to expect substantial variation in the gas properties of clusters, independently of their dark matter distribution. Models that seek to account for the mean M-L and M-T relations require some form of entropy modification in the central regions of the systems (Thomas et al. 2002; Viana et al. 2003). Pure heating models have been very successful in explaining the average trends of these scaling relations, especially when the heating targets the lowest entropy gas (Kaiser 1991; Balogh et al. 1999; Babul et al. 2002, hereafter BBLP). It seems likely that the efficiency of whatever physical mechanism is responsible for the heating (e.g. heat transport, AGN energy injection, etc) will vary from cluster to cluster. In this case, one expects both cooling and the feedback it triggers to eliminate gas below an entropy threshold that depends on halo mass and redshift (Voit & Bryan 2001; Voit et al. 2002, hereafter VBBB), although some gas may exist below this threshold if it is in the process of cooling out. In a realistic cooling model (e.g. McCarthy et al. 2004), scatter can be introduced by appealing to a range in time available for cooling in each halo. Despite this, McCarthy et al. show that such a range alone cannot account for the scatter in the M-L relation; it is also necessary to introduce variations in an initial heating level. However, they do not consider the effect of variations associated with the underlying dark matter potential, which will contribute some scatter independently of the gas entropy distribution.

Shorter-lived changes to the equilibrium temperature and luminosity of a cluster may also be associated with merger events (e.g. Ritchie & Thomas 2002; Randall et al. 2002; Rowley et al. 2004). Departures from equilibrium in the potential can change the luminosity, but have little effect on the gas temperature (Rowley et al. 2004). However, the shocks associated with mergers can have a temporary but significant influence on both the temperature and luminosity of the gas (Ritchie & Thomas 2002; Rowley et al. 2004).

Recently, semi- and fully-numerical simulations which include both cooling and feedback from star formation have been shown to produce clusters with X-ray properties that scale with mass in a way that is in reasonable agreement with the observations (e.g. Muanwong et al. 2001; Thomas et al. 2002; Borgani et al. 2002; Viana et al. 2003; Kay et al. 2004; Rowley et al. 2004; Borgani et al. 2005; Ostriker et al. 2005). In this paper we will re-examine the observed M-L and M-T relations, focusing on the scatter in these relations and how it relates to the expected varia-

tion in the underlying physical processes. The data we use are uncorrected for any cooling-core component, since it is precisely this core region that interests us. We will compare these observations with analytic, hydrostatic models which allow modifications to the entropy distribution of the gas (BBLP, VBBB), to determine the range of model parameters that are required to reproduce the observed scatter. Although the hydrostatic nature of these models means they are not ideally suited to explore in detail the effects of active cooling or heating in clusters, the range of model parameters required to match the data can be related indirectly to these processes. We will also make a self-consistent comparison with the temperature and luminosity functions, which provide an independent test of the models assuming the dark matter mass function is known (Evrard et al. 2002). Finally, we will present the redshift evolution of all these observable quantities to put further constraints on the model parameters.

Throughout this paper we use a cosmology with $\Omega_m = 0.3$, $\Omega_\Lambda = 0.7$ and $H_0 = 70 \text{ km s}^{-1} \text{ Mpc}^{-1}$. The theoretical models are described in § 2, and the comparison with observed X-ray properties is presented in § 3. Predictions for the evolution of these models, and some comparison with early data, are given in § 5. We summarize our conclusions and discuss the implications and limitations of our findings, in § 6.

2 THE MODELS

2.1 Dark matter profile shapes

The average theoretical shapes of dark matter halos are well motivated by N-body simulations to have a form given by

$$\rho \propto r^{-n_1} (1 + c_{200} r)^{-n_2} \quad (1)$$

(Navarro et al. 1996, NFW), where n_1 , n_2 , and c_{200} are fitting parameters. The primary determinant of a halo's structure is its virial mass, M_{vir} . This is commonly defined, using spherical collapse models, as the mass within a fixed overdensity Δ that depends on cosmology and redshift; for ΛCDM , $\Delta \sim 100$ at $z = 0$ (Eke et al. 1996). However, observations are more typically made at $\Delta = 200, 500$ or larger. The radius and mass corresponding to the overdensity Δ will be denoted R_Δ and M_Δ , respectively.

High resolution simulations show that relaxed clusters have remarkably uniform profiles. We will assume an NFW profile with $n_1 = 1$ and $n_2 = 2$ as our fiducial model. The range of values of these parameters reported in the literature (e.g. Moore et al. 1998; Lewis et al. 2000) appear to be mostly due to differences in resolution and the fact that the fitting formula is not a perfect description of the profile (Hayashi et al. 2004). Within a given simulation, an indication of the amount of variation in halo shapes is best given by the distribution of concentration parameters, c_{200} . This parameter has a systematic dependence on mass and redshift (e.g. Eke et al. 1998; Bullock et al. 2001; Power 2003; Wechsler et al. 2002); we will take the parameterization of Eke et al. (2001), assuming $\sigma_8 = 0.8$. Most importantly for our purposes, c_{200} shows considerable scatter at fixed mass and redshift; Dolag et al. (2004) have recently shown that the distribution of c_{200} values in simulated clusters (selected

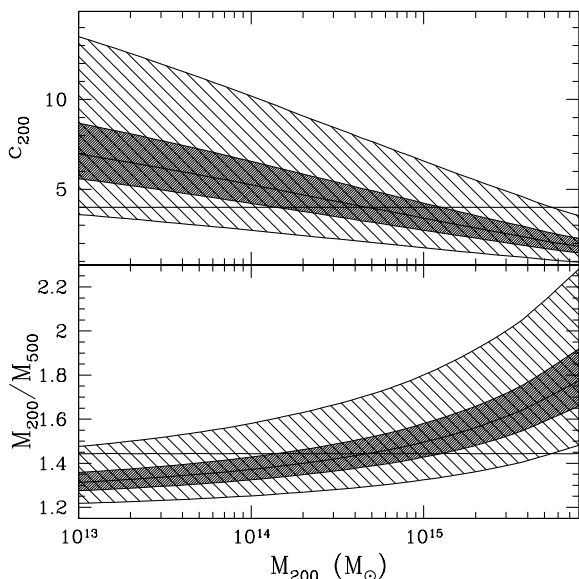


Figure 1. Top panel: The relation between c_{200} (concentration) and M_{200} as a function of M_{200} is shown as the shaded region, where the distribution is due to the $1 - \sigma$ (heavy shading) and $3 - \sigma$ (light shading) distribution of concentrations from Dolag et al. (2004). The horizontal line shows a fixed concentration of 4, for reference. **Bottom panel:** The relation between M_{500} and M_{200} as a function of M_{200} is shown as the shaded region, assuming the same distribution of concentrations above. The horizontal, solid line shows the result for a model with a fixed concentration, $c_{200} = 4$.

only based on an overdensity criterion) is approximately log-normal with a width that is nearly independent of mass. This scatter is at least partly due to the presence of sub-structure, triaxiality, and departure from equilibrium in the sample of simulated clusters chosen from the simulations. We will therefore consider a range of concentrations corresponding to the $\pm 3\sigma$ range predicted from this distribution. Although different values of σ_8 will change the value of c_{200} at fixed mass by a small amount, it will not have an important effect our discussion in this paper, which is based on the variation in c_{200} and not its absolute value.

In Figure 1 we show how the concentration and its scatter depend on dark halo mass M_{200} in our model. The average concentration and its scatter both decline with increasing mass. In the bottom panel we show how this affects the ratio M_{200}/M_{500} . The scatter in concentration at a fixed mass corresponds to a ~ 10 per cent scatter in M_{200}/M_{500} . The dependence of concentration on mass means the slope of measured correlations between observables (like X-ray temperature and luminosity) and mass will depend on which mass is used. Throughout this paper we will present our results as a function of M_{200} , and this relation can be used to deduce the corresponding value of M_{500} .

2.2 Entropy distributions

The shape of the gas profile in a cluster of given mass is determined by the entropy distribution of that gas, which is sensitive to its thermodynamic history. We adopt the

common (e.g. Ponman et al. 1999) redefinition of entropy as $K \equiv kT_e n_e^{-2/3}$, where T_e and n_e are the electron temperature and density, respectively. This is related to the thermodynamic entropy by a logarithm and an additive constant, and is given in units of keV cm 2 . We will usually quote this quantity in dimensionless units, relative to $K_{100} = 100 \text{ keV cm}^2$.

We use the formalism of VBBB to compute the hydrostatic equilibrium gas distributions under different assumptions about the dark matter potential and the thermodynamic history of the gas. Once the halo potential is specified, the entropy distribution and appropriate boundary conditions are all that are required to fully describe the gas density and temperature profiles. We start with an initial profile where the gas density traces the dark matter density, and solve for the temperature profile needed to satisfy the assumption of hydrostatic equilibrium. This is a good approximation at large radii, where the entropy scales approximately as $K \propto r^{1.1}$, as found from analytic modelling and numerical simulations (Lewis et al. 2000; Tozzi & Norman 2001; Voit et al. 2003; McCarthy et al. 2005). The gas distribution at smaller radii is dominated by the entropy modifications that we discuss below, so the choice of initial profile is relatively unimportant. The normalization of this initial, unmodified model, is chosen by assuming the gas fraction within R_{200} is equal to the global baryon fraction of 12.9 per cent (for $h = 0.7$ and $\Omega = 0.3$, Burles et al. 2001; Spergel et al. 2003).

We will explore modifications to this default profile, in the form of the shifted-entropy models of VBBB. In this case, the entropy distribution is shifted by an additive constant, which provides a good approximation to pre-heated models. This entropy shifting causes the gas to expand beyond R_{200} ; following VBBB we therefore choose as our pressure boundary condition the accretion pressure at the maximum radial extent of the gas. The amount by which the entropy distribution is shifted will be left as a free parameter; for our base model we use $K_o = 2K_{100}$, which is known to provide a reasonable match to the median global scaling relations of clusters (McCarthy et al. 2004).

We will also consider the case where K_o is set by the entropy of gas that can efficiently cool in time t . This entropy, which we will call K_{cool} , depends on mass and redshift (Voit & Bryan 2001), but also on the time available for cooling (McCarthy et al. 2004). Figure 2 shows the maximum value of K_o predicted in this cooling-based model, calculated assuming the gas can cool for a Hubble time. The mean value of K_{cool} decreases with increasing redshift due primarily to the decrease in time available for cooling. Of course, simply shifting the entropy distribution by a constant value is not an accurate representation of the effects of radiative cooling. In reality, an inner entropy gradient (rather than a floor) may be expected, with some gas below the entropy threshold (VBBB; McCarthy et al. 2004). This can be particularly important for clusters, where the central entropy in a more realistic model can drop well below the value of K_{cool} . Furthermore, the time available for cooling will likely vary from cluster to cluster, but must always be less than a Hubble time. Both of these effects tend to reduce the value of K_o ; thus our prediction in Figure 2 represents a strict maximum value for this quantity.

It is important to note that the entropy modifications

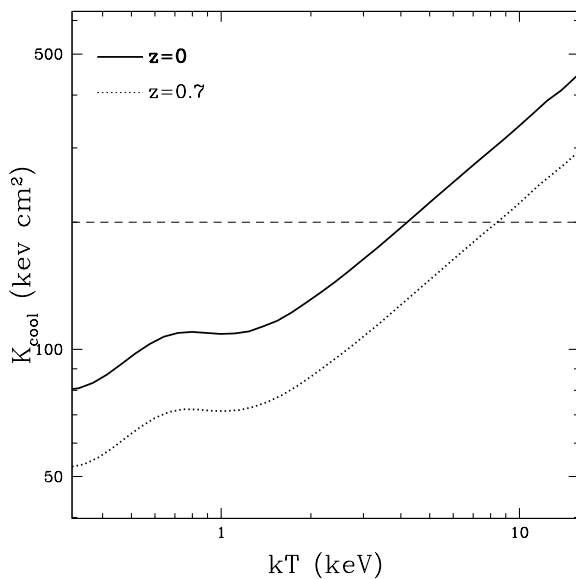


Figure 2. The entropy K_{cool} corresponding to the maximum entropy for gas that can cool in a Hubble time, as a function of halo virial temperature and redshift. The horizontal, *dashed line* shows the $K_{\text{cool}} = 2K_{100}$ line for reference.

that we explore in the present study are all confined to the cluster core. Therefore, our approach is to effectively bracket the range of central entropy levels required for the heating-based and cooling-based models to explain the scatter in the observational data. Both models implicitly assume that the entropy distribution at large radii is essentially identical to that found in clusters formed in cosmological numerical simulations. Gas at large distance from the centre is not easily affected by cooling or non-gravitational heating processes once the cluster is assembled (e.g. Borgani et al. 2005; Ostriker et al. 2005). However, heating of the gas before it is accreted into a cluster can smooth out the density distribution of infalling gas, and this increases the entropy jump at the accretion shock (Voit et al. 2003; Borgani et al. 2005). In this case, the entropy distribution at large radii will be larger than that we have assumed, and a lower value of central entropy will be required to explain the observations. This underscores the need for detailed comparisons of theoretical models to the spatially-resolved entropy distributions of large, representative samples of clusters. At present, however, only a relatively small number of clusters have accurately-determined entropy profiles from *Chandra* and *XMM-Newton* data. Analysis of this small dataset seems to confirm that for high mass clusters ($kT \gtrsim 4$ keV) the entropy distribution at large radii does indeed trace the spatial distribution and normalization predicted by ‘adiabatic’ hydrodynamic simulations (McCarthy et al. 2004). This conclusion is strengthened by the fact that for high mass clusters there also appears to be excellent agreement between the observed projected temperature profiles at large radii and those predicted by hydrodynamic simulations (e.g., De Grandi & Molendi 2002; Loken et al. 2002; Vikhlinin et al. 2005). Thus, our estimates of K_0 for such systems should be robust. However, for cooler systems, there are preliminary indications of excess entropy at large radii

(e.g., Ponman et al. 2003; Pratt & Arnaud 2005). As such, our estimates of K_0 for low temperature systems should be treated with some caution. In this paper, our conclusions rest primarily on the data for the high mass clusters.

2.3 Prediction of observable quantities

To compute X-ray observables from the analytic gas profiles we use the cooling functions of Raymond et al. (1976) for gas with one third solar metallicity. To avoid the need to make bolometric corrections to the data, which depend on an accurate measurement of the gas temperature, we compute the model luminosities within the observed *ROSAT* energy bands 0.1–2.4 keV and 0.5–2.0 keV. Total luminosities are obtained by integrating out to a minimum surface brightness of 1×10^{-15} ergs s^{-1} cm^{-2} arcmin^{-2} , similar to that of the WARPS survey (Scharf et al. 1997), unless stated otherwise¹. The sensitivity of our results to this limit are explicitly noted.

The model temperatures we compute are emission-weighted by the 0.1–2.4 keV luminosity, again excluding regions below the WARPS surface brightness limit; however the choice of energy band and surface brightness limit have a negligible effect on the calculated temperatures for our purposes. Simulations suggest that spectral temperatures, as measured observationally, can be 10–20 per cent higher than emission-weighted temperatures (Mathiesen & Evrard 2001; Rasia et al. 2005; Vikhlinin 2005). For relaxed clusters, the difference is probably closer to the lower end (~ 10 per cent) of this range (Rasia et al. 2005). However, this systematic error is not of major concern for the present study, as the statistical errors associated with the observed temperature, mass, and luminosity of a given cluster are typically twice as large as this. For example, in McCarthy et al. (2004) we derived similar constraints on the parameters of heating and cooling models of the intracluster medium (ICM) from independent analyses of the M–L and luminosity–temperature (L–T) relations, which suggests that small systematic errors in temperature measurements do not have a noticeable influence on our results.

Our primary source of data is the HIFLUGCS cluster sample (Reiprich & Böhringer 2002). This survey is an X-ray flux-limited sample of nearby clusters based on the *ROSAT* All Sky Survey, in which cluster masses are determined from the density profiles, assuming hydrostatic equilibrium and isothermal temperature profiles. It is common practise when considering X-ray scaling relations to use temperatures and luminosities that are corrected for a cooling flow component, and it is known that this reduces the scatter in these relations (e.g. Markevitch 1998). However, since it is precisely this scatter that is the focus of our study, we will present all the data as observed, without this correction. We take these raw cluster luminosities, in the 0.1–2.4

¹ We note that Scharf et al. (1997) attempt to correct for flux below the surface brightness limit. However, the flux correction to the data (typically a factor ~ 1.4) is an underestimate at the lowest luminosities, since it assumes a surface brightness profile slope of $\beta = 0.67$, appropriate for high and moderate luminosity clusters but not for low luminosity groups. Thus, the lowest luminosity data points may still systematically underestimate the luminosities by a factor $\lesssim 2$.

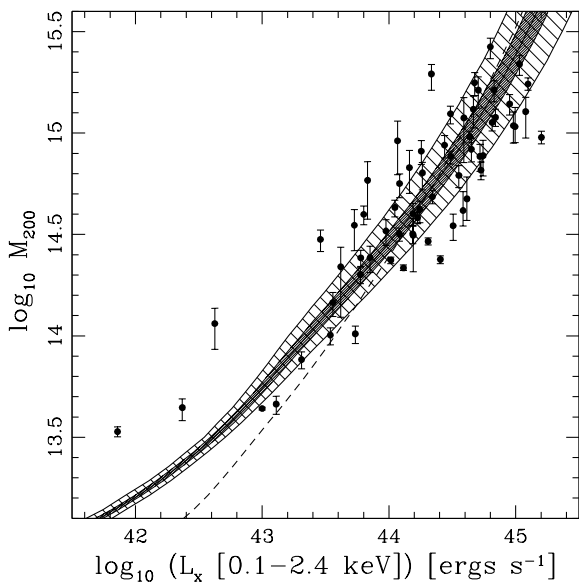


Figure 3. The relation between X-ray luminosity in the 0.1–2.4 keV band and halo mass M_{200} . The filled circles are local ($z < 0.2$) data from the HIFLUGCS sample (Reiprich & Böhringer 2002). 1– σ error bars on the masses are shown; only clusters with relative errors of < 50 per cent are plotted. The shaded region shows the shifted entropy model with $K_o = 2K_{100}$ and a 1 σ (heavy shaded region) and 3 σ (lighter shaded) range of halo concentrations. The dashed line represents the model with $K_o = K_{\text{cool}}$, using the most probable value of c_{200} at each mass.

keV band, from the Reiprich & Böhringer (2002) catalogue. Since many of the temperatures and masses in this catalogue have been subjected to a significant cooling-flow correction, we will only keep the ~ 80 clusters (out of 106) for which uncorrected temperatures are available, from the catalogue of Horner (2001). The dynamical mass estimates, M_{200} and M_{500} , are derived from the gas temperature, assuming hydrostatic equilibrium. To be fully consistent, we make a small adjustment to these masses ($M \propto T$) so they agree with the original (uncorrected) temperatures.

3 SCATTER IN THE M-T AND M-L SCALING RELATIONS

3.1 The M-L relation

In Figure 3 we present the M-L relation from the data of Reiprich & Böhringer (2002), excluding those clusters with mass uncertainties greater than 50 per cent. Note that the mass we plot here is M_{200} . Observationally, M_{500} can be more precisely determined, and this can reduce the purely observational scatter in this Figure (Rowley et al. 2004). However, when we construct the temperature and luminosity function in § 4 we will have to use M_{200} , since this was the mass used to derive the mass function from numerical simulations (Evrard et al. 2002). For consistency, therefore, we have used M_{200} throughout the paper. We show both observed and model luminosities in the 0.1–2.4 keV band, to minimize errors in bolometric corrections to the observations. The limiting surface brightness cut applied to the

models (see § 2) results in a significant reduction of luminosity only below $M_{200} \sim 10^{13.5} M_{\odot}$. The shifted-entropy model reproduces the slope and normalization of the relation well. However, the scatter in the data is much larger than expected from the observational uncertainties, as has been noted before (e.g. Fabian et al. 1994; Markevitch 1998).

Our calculations show that the observed scatter is much larger than can be expected from variations in halo concentration. This is shown by the shaded region in Figure 3, which represents the 1– and 3– σ range of luminosities predicted at a given mass, from the dispersion in simulated cluster concentrations alone. Approximately 25 per cent of the observed clusters lie well outside the 3 σ range resulting from variations in halo concentration. Even though our models assume spherical, smooth, virialized halos, these effects are partly accounted for by the variation in concentration parameter, which is determined from simulated clusters that are clumpy, non-spherical and in a variety of dynamical states. Furthermore, the predicted scatter in the scaling relations is not significantly larger in models which consider more realistic potential shapes (Rowley et al. 2004; Ostriker et al. 2005). It is therefore unlikely that the observed scatter in this relation can be entirely attributed to variations in the shape of the dark matter distributions.

Some of the scatter in the M-L relation could be due to short-timescale events like mergers, which cause changes in both the luminosity and temperature of the gas (e.g. Ritchie & Thomas 2002; Randall et al. 2002; Rowley et al. 2004). However, it has been shown that these changes tend to move galaxies along the L-T relation, and do not contribute significantly to its scatter; since the observational scatter in the L-T relation is comparable in magnitude to that in the M-L relation of Figure 3 (Fabian et al. 1994; Markevitch 1998), there must be an important source of scatter other than mergers. Furthermore, as major mergers in massive clusters are expected to have been relatively rare in the past ~ 2 Gyr (e.g. Kauffmann & White 1993; Lacey & Cole 1994), and the luminosity and temperature boosts typically last for ~ 0.5 Gyr or less following a major merger, these events are relatively rare and unlikely to be responsible for all the observed scatter in an unbiased cluster sample.

On the other hand, the X-ray luminosity of a cluster of given mass is very sensitive to the entropy floor level, as shown in Figure 4. A range of entropy levels 0.5–5 K_{100} approximately covers the scatter in the observations, at high masses. For a few clusters even higher levels of $K_o \approx 7K_{100}$ are required to match their low luminosities, something that was also observed in our earlier comparison with Sunyaev–Zeldovich measurements (McCarthy et al. 2003). This is a remarkably large range in central entropy levels, and thus substantial variations in heating or cooling efficiency must exist from cluster to cluster, even if some of the observed scatter can be attributed to substructure, departures from equilibrium, or merger-induced shocks.

In the cooling-based model, the entropy floor is related to the cooling time (as in Figure 2). This model predicts that K_o depends on mass, increasing by a factor of ~ 5 from $\sim 0.8K_{100}$ to $\sim 4K_{100}$ over the temperature range of interest. The resulting M-L relation is shown as the dashed line in Figure 3; the slope here is steeper than for any of the fixed entropy-floor models shown in Figure 4. Note, however, that

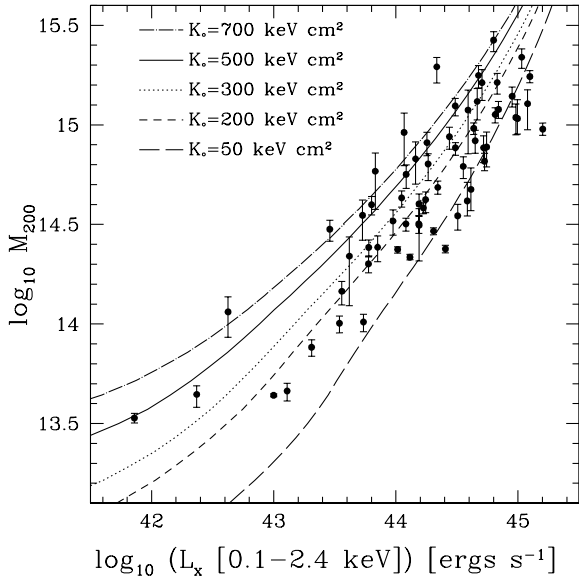


Figure 4. The mass–luminosity relation, with data as in Figure 3, and five models of fixed concentration but different entropy thresholds, as labelled.

while K_o may vary by a factor of ~ 5 over this mass range, a similar or larger range of K_o is required to explain the distribution of luminosities at fixed mass. Although the cooling model can easily accommodate scatter toward more luminous clusters (since K_{cool} is only the maximum entropy of gas that can cool), there is no simple mechanism to account for the scatter of clusters toward lower luminosities. Therefore the simple interpretation that the entropy threshold is due solely to the cooling of low entropy gas is not likely to be correct, a conclusion also reached by McCarthy et al. (2004) and Borgani et al. (2005) using more sophisticated models that account for the presence of gas that cools below the K_{cool} threshold.

3.2 The M-T relation

In Figure 5 we compare the mass-temperature relation predicted by our models with the Reiprich & Böhringer (2002) catalogue, again excluding those clusters with mass uncertainties greater than 50 per cent, and using temperatures from Horner (2001). The shifted-entropy model provides a good description of the data over two orders of magnitude in mass, although it is not statistically the best fit.

Unlike the M-L relation, the observations here show remarkably little scatter, and this scatter is consistent with the published measurement uncertainties. Recently, Smith et al. (2005) used strong gravitational lensing to measure the masses of ten X-ray luminous clusters and found that there is intrinsic scatter in the M-T relation, due mostly to merging, non-equilibrium systems. Although this scatter is not apparent in Figure 5, it is possible that it is underrepresented here, as M_{200} is obtained from the X-ray data by assuming isothermality and imposing a functional form for the surface brightness profile (Rasia et al. 2005). This parametrization could have the effect of homogenizing clusters with a range of cooling core sizes, geometries, and amount of substructure.

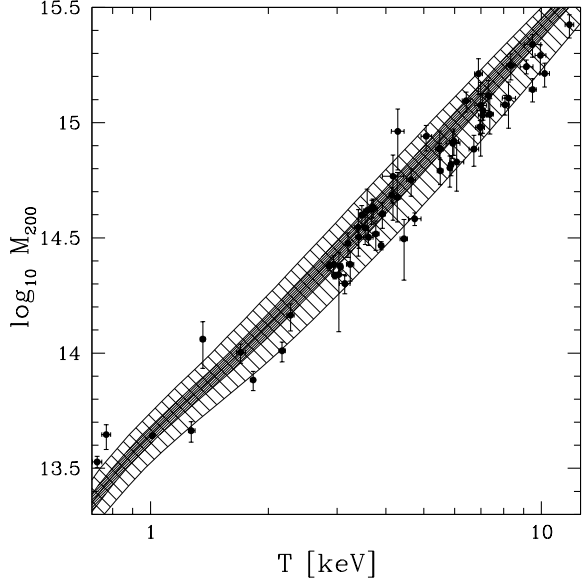


Figure 5. The relation between X-ray temperature and M_{200} . The *points* are local ($z < 0.2$) data, with masses from the HI-FLUGCS sample (Reiprich & Böhringer 2002) and temperatures (uncorrected for cooling flows) from Horner (2001). $1-\sigma$ error bars on the masses are shown; only galaxies with relative errors of < 50 per cent are plotted. The *shaded region* represents the prediction of the shifted-entropy model with $K_o = 2K_{100}$ and a realistic 1σ (heavy shading) or 3σ (lighter shading) scatter in the halo concentration parameter.

The same would also be true for the masses in the M-L relation, where we do see significant scatter (Figure 3), and this could indicate that the intrinsic scatter in the luminosities is larger than the intrinsic scatter in the temperatures. On the other hand, the fact that X-ray derived masses are directly proportional to the temperature introduces a correlation that could reduce the scatter in the M-T relation alone. It would be useful to have a larger sample of clusters with accurate lensing masses and X-ray observations to improve our understanding of the scatter in these relations.

The model predictions in Figures 5 and 6 show that the predicted temperature is relatively insensitive to both the halo structure (i.e. concentration) and the entropy floor, for $K_o > 0.5K_{100}$. Recall that the distribution of halo concentrations partly arises from substructure, triaxiality and departures from equilibrium in simulated clusters and therefore our predicted scatter approximately includes these effects. However, in our model these concentrations are applied to spherical, smooth halos and the scatter in predicted temperatures is therefore not as large as in numerical and analytic models that do not make these assumptions (Rowley et al. 2004; Ostriker et al. 2005). The insensitivity of our predicted temperatures to the value of the entropy floor is due to the fact that the higher central temperature associated with larger K_o is offset by the flattening of the central density profile, which means the luminosity-weighted temperature is dominated by the temperature at larger radius. Thus, even a model with $K_o = 0.5K_{100}$ predicts temperatures that are just within the scatter of the observations. For the same reason, the K_{cool} model predic-

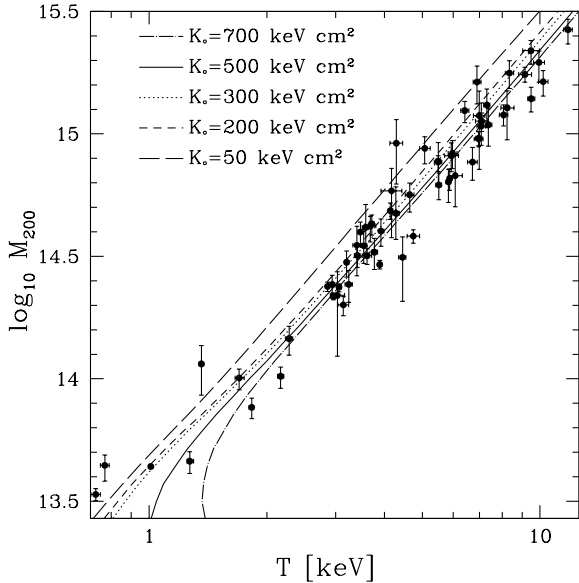


Figure 6. As Figure 4, but for the mass–temperature relation.

tion does not differ significantly from those shown here, so we have omitted it from the figure for the sake of clarity.

In summary, we have found that a variation of nearly an order of magnitude in K_o is required to explain the large scatter in the $M - L$ relation. Variations in dark matter halo shape (concentration) alone are insufficient. Encouragingly, the wide range of entropy levels required does not conflict with the small observed scatter in the $M - T$ relation, because of the temperature’s insensitivity to the core properties. Although both theory (e.g. Rowley et al. 2004; Ostriker et al. 2005) and observations (Smith et al. 2005) suggest that there may be additional scatter in the M-T relation that is not apparent under the simplifying assumptions of both the models and data presented here, it is still less than the scatter in the M-L relation, which is dominated by variations in the entropy distribution of the gas.

4 SCATTER AND THE LUMINOSITY AND TEMPERATURE FUNCTIONS

If the mass spectrum of dark matter halos is known precisely, then the observed shape and normalization of the temperature and luminosity functions provides an independent test of the theoretical models, that does not depend on an observational determination of cluster mass. Scatter in the mean relations plays an important role here, and can influence the shape of these functions.

We construct the theoretical luminosity and temperature functions using the dark matter mass function of Evrard et al. (2002), based on the fitting formalism of Jenkins et al. (2001), which provides a universal description of the mass function to within about 10 per cent. The advantage of the Evrard et al. (2002) mass function is that it is expressed in terms of M_{200} , the same mass that we use to compare with the observed mass-temperature and mass-

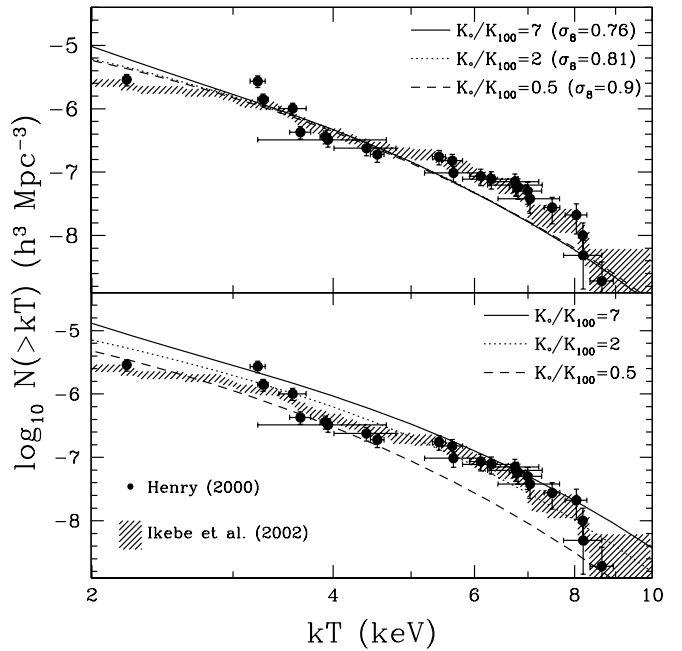


Figure 7. The shaded region is the observed temperature function at $z = 0$ from Ikebe et al. (2002), but with temperatures, uncorrected for cooling flows, taken from Horner (2001). The data points are from Henry (2000). In the bottom panel we show the shifted-entropy model with three different levels of heating, assuming $\sigma_8 = 0.85$ as determined from WMAP (Spergel et al. 2003; Tegmark et al. 2004). Models are convolved with a 10 per cent uncertainty in temperature which flattens the temperature function. In the top panel, we show the same models, normalized at 4–5 keV with different values of σ_8 , as indicated.

luminosity relations². The form of the temperature and luminosity functions are then completely determined by the correlation between virial mass and the X-ray observable (BBLP³).

4.1 The temperature function

The observed $z = 0.15$ temperature functions from Ikebe et al. (2002) and Henry (2000) are shown in Fig. 7. For consistency, the temperatures are taken from Horner (2001), and therefore uncorrected for any cooling flow component, though this makes little difference in practise. To compare with these data, we show predicted temperature functions from the shifted-entropy models with a range of normalizations that approximately accounts for the scatter in the M-L relation. We have smoothed the models with 10 per cent Gaussian random noise on the temperatures, to mimic the scatter in the mean relation (which is consistent with being due to observational uncertainties). First, in the bottom panel, we show three models with different K_o

² We note that M_{500} is better determined observationally, and it would be useful to have a mass function from numerical simulations filtered on this scale.

³ However, both the observed and model luminosity functions shown in Figure 9 of BBLP are incorrect due to errors in the bolometric correction and cosmology conversion.

but the same normalization $\sigma_8 = 0.85$, as measured from the WMAP data (and adjusted for the slightly non-concordance values of cosmological parameters that we have adopted Spergel et al. 2003; Tegmark et al. 2004). At the hot end of the temperature function, the data is best matched by the models with the highest entropy floors, while at the opposite extreme the low-entropy models fare better. However, we caution that at low temperatures ($\lesssim 1$ keV) there may be completeness issues that could artificially flatten the temperature function and, therefore, yield values of K_\circ that are systematically lower than that of the average system (e.g. Osmond & Ponman 2004).

In the top panel of Fig. 7, we again show the predicted temperature functions for a range of K_\circ values, but with σ_8 adjusted to give the same number density of clusters at $T = 4\text{--}5$ keV, where observational data from different studies are in best agreement (Ikebe et al. 2002). The best-fit value of σ_8 is ~ 3.5 per cent higher if the normalization to the data is made over the range $kT = 6\text{--}7$ keV. The range of K_\circ (which are all reasonably consistent with the mass-temperature relation) corresponds to a range of best-fit values of σ_8 ranging from 0.76 to 0.9. This is comparable to the observational uncertainty on this parameter (Spergel et al. 2003), and therefore we cannot use the temperature function alone to provide a sensitive test of the size of the entropy floor. This is again simply because temperature is relatively insensitive to the entropy of the central gas.

4.2 The Luminosity Function

To compute the luminosity function, the intrinsic scatter in the M-L relation must be taken into account. Because of the steepness of the mass function, even a small distribution of halo masses corresponding to a given luminosity can have an important effect on the number density of clusters at that luminosity. Unfortunately, the value of K_\circ in our model does not have a unique physical motivation, and thus we do not have a prediction for the scatter as a function of mass. However, we can see from the data in Figure 3 that the observations are approximately covered by models with a range of entropy floors $0.5 < K_\circ/K_{100} < 7$, so in Figure 8 we show the prediction of the luminosity function for these two extremes. The true luminosity function should lie between these limits, with a shape that depends on the distribution of entropy levels at each luminosity.

The observed luminosity functions at $z = 0.15$ from the WARPS (Jones et al. 2001, Jones et al., in prep.) and REFLEX (Böhringer et al. 2001) surveys are shown in Figure 8. The solid lines show our model, for $K_\circ = 0.5K_{100}$ (upper line) and $K_\circ = 7K_{100}$ (lower line). This range brackets the observational data, although the data do lie nearer the model with high entropy. This is especially true for the low-luminosity clusters, with $L \lesssim 10^{44}\text{ergs s}^{-1}$. This may indicate that lower-mass clusters have higher central entropies, on average; this may also be evident from Figure 3, although there are few clusters with accurate mass measurements at these low luminosities.

We also show, as the dotted lines, the effect of varying σ_8 between 0.76 and 0.9 (assuming $K_\circ = 2K_{100}$). This has only a small effect on the bright end of the luminosity function, and no effect on the faint end. The dashed line shows the effect of removing the limiting surface brightness

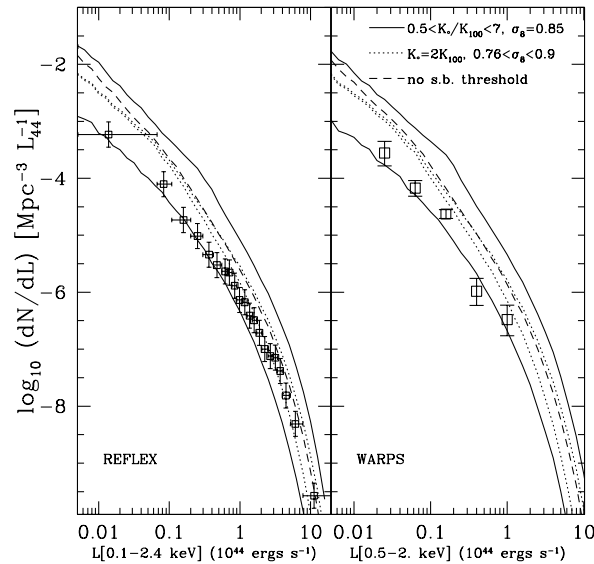


Figure 8. The lines in each panel show different theoretical models for the luminosity function. The *solid lines* show models with entropy floors of $K_\circ = 0.5K_{100}$ (upper line) and $K_\circ = 7K_{100}$ (lower line). This approximately brackets the range of entropies required to explain the scatter in the M-L relation (Figure 3). The *dotted lines* show the effect of varying σ_8 as indicated, keeping $K_\circ = 2K_{100}$ fixed; lower values of σ_8 reduce the number of luminous clusters by a small amount but have no effect on the faint end of the luminosity function. Finally, the *dashed line* shows the $K_\circ = 2K_{100}$ model but omitting the surface brightness threshold, which increases the prediction at low luminosities. *Left panel:* The *open squares* with error bars are the observed local luminosity function from the REFLEX survey (Böhringer et al. 2001). *Right panel:* Similar, but where the data are from the WARPS (Jones et al. 2001, Jones et al., in prep.), in a different energy band.

threshold of $1 \times 10^{-15}\text{ ergs s}^{-1}\text{ cm}^{-2}\text{ arcmin}^{-2}$ (Scharf et al. 1997) used in the other models; these surface brightness corrections are relevant only for the least luminous clusters in the sample.

Thus we have shown that consistency between the X-ray scaling relations (M-L and M-T) and the luminosity function can be achieved in these models; however, a better understanding of the entropy-floor distribution as a function of mass is required to make a firm prediction of the luminosity function shape.

5 EVOLUTION

We now turn to the redshift evolution of the X-ray scaling relations and the temperature and luminosity functions. These predictions can provide another interesting test of the difference between the fixed- K_\circ , preheating models and models where $K_\circ = K_{\text{cool}}$.

In Fig. 9 we show the predicted evolution in the mass-temperature and mass-luminosity relations for the two models. The data are the same $z \sim 0.15$ data shown in Figures 3 and 5, and the model predictions are shown at $z = 0, 0.15, 0.4$ and 0.7 . For massive clusters, $T \gtrsim 4$ keV,

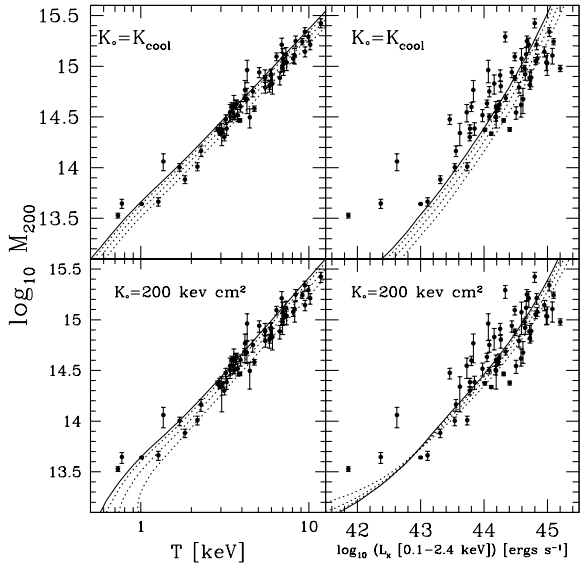


Figure 9. The observed M–L and M–T relations shown in Figs. 3 and 5 are reproduced as the *solid circles*. In the *bottom panels* we show the default model predictions, where the entropy floor is independent of redshift, at $z = 0$ (*solid line*) and $z = 0.15, 0.4, 0.7$ (*dotted lines*). The curves in the *top panels* are the models where the entropy floor K_{cool} is related to the cooling time of the gas and thus evolves with redshift.

the predicted evolution in both the M–T and M–L correlations is mostly in the normalization, with little change in the slope.

The amount of evolution in the M–L relation is small relative to the observed scatter at $z = 0$. On the other hand predicted evolution in the M–T relation is more noticeable; clusters at a given temperature are predicted to be 40–60 per cent less massive at $z \sim 0.7$. The sense and magnitude of the evolution are comparable to recent *XMM-Newton* and *Chandra* data (Kotov & Vikhlinin 2005; Maughan et al. 2006). Both the $K_{\text{o}} = 2K_{100}$ and the $K_{\text{o}} = K_{\text{cool}}$ models predict a similar amount of evolution for the $M - T$ relation, so this is not a useful way to discriminate between them.

Interestingly, although the evolution in the M–T and M–L relations appear similar for both models, the predicted evolution of the L–T scaling law is in opposite directions, as shown in Figure 10. At high temperatures, the amount of evolution in the predicted relation is very small. For the fixed-floor model, the evolution is negligible, while the K_{cool} model predicts that high redshift clusters will be about 30 per cent more luminous at fixed temperature, due to the fact that the entropy floor is lower at higher redshift. Observations of distant clusters seem to indicate a much stronger evolution, with clusters at $z \sim 0.7$ being up to 2.5 times brighter than local clusters of the same temperature (Vikhlinin et al. 2002; Lumb et al. 2004; Kotov & Vikhlinin 2005; Maughan et al. 2006). In principle, this observation has the potential to rule out both models shown here. However, we note that the amount of evolution observed is sensitive to the details of the analysis (e.g. Ettori et al. 2004a,b). Since any evolution in the mean scaling relation is much less

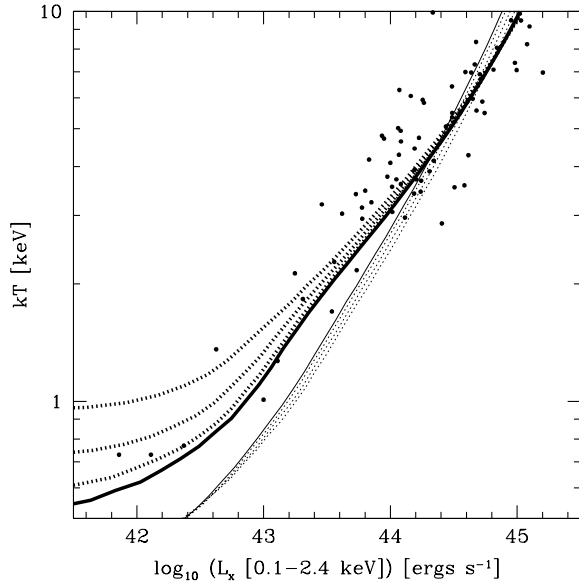


Figure 10. The observed temperature–luminosity relation at $z = 0$ is shown as the *solid circles*. The *thin* and *thick* lines represent the K_{cool} and $K_{\text{o}} = 2K_{100}$ models, respectively. Predictions are shown for $z = 0$ (*solid line*) and $z = 0.15, 0.4, 0.7$ (*dotted lines*).

than the factor ~ 4 scatter in luminosity at fixed temperature for local clusters, it is probably premature to claim these observations rule out either model until the scatter and the selection biases that result from it (i.e. Malmquist-like bias) are robustly integrated into the model predictions. The most leverage will come from low temperature systems at high redshift; the $K_{\text{o}} = 2K_{100}$ model predicts very strong (negative) evolution in the luminosities of these groups, as the fixed entropy floor becomes very large relative to the characteristic entropy.

The evolution of the temperature and luminosity functions requires a knowledge of the mass function at $z > 0$. Since this has not yet been precisely measured from simulations, we take the local mass function from Evrard et al. (2002) and evolve it to higher redshift using Press-Schechter theory. In Figure 11 we show the temperature function for both models (normalized at $kT \sim 4-5$ keV, with $\sigma_8 \sim 0.8$), at $z = 0, 0.4$ and $z = 0.7$, compared with $z = 0.4$ data from Henry (2000)⁴. Over the range of observed temperatures, $kT > 3$ keV, the evolution in the two models is similar, and in good agreement with the observations. The models begin to diverge at lower temperatures, where the fixed-entropy model predicts a little less evolution.

The predicted evolution of the luminosity function is shown in Figure 12. Unfortunately, our model does not predict the scatter in the M–L relation nor its evolution, so for illustration we have just shown the $K_{\text{o}} = 2K_{100}$ model, which provides a reasonable match to the bright end of the local luminosity function. The models are again compared with data at similar redshifts, from the WARPS survey (Jones et al. 2001, Jones et al., in prep.). The WARPS data

⁴ An updated version of the observed high-redshift temperature function, based on more data, is presented in Henry (2004). The results are consistent with those shown here.

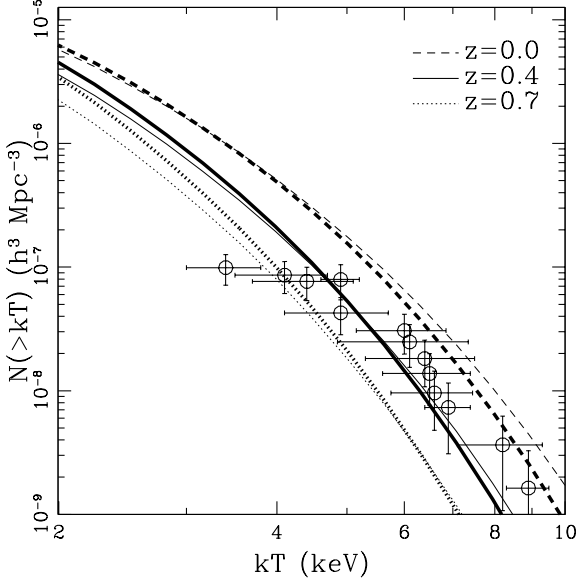


Figure 11. The predicted temperature functions at $z = 0, 0.4$ and $z = 0.7$, for the fixed-entropy models (thick lines) and the K_{cool} models (thin lines). The data are at $z \sim 0.4$, from Henry (2000).

at $z > 0.6$ have been updated with accurate luminosities measured from XMM-Newton and Chandra observations, and are corrected to the rest-frame energy range 0.5–2.0 keV. In contrast with the temperature function, the observed luminosity function evolution is modest, with a factor ~ 3 decrease in the number of massive clusters between $z = 0$ and $z = 0.7$.

The K_{cool} model predicts very little evolution in the luminosity function, and thus overpredicts the number of high redshift clusters. The $K_{\odot} = 2K_{100}$ model appears to be in much better agreement with the data, especially for the brightest clusters. As with the local luminosity function, the disagreement at the faint end may indicate that lower luminosity clusters have larger central entropies. However, as we have already seen (Figure 8), the shape of the luminosity function is very sensitive to the amount of scatter in the M–L relation, and we have no theoretical or empirical knowledge about how this scatter evolves. We also note that the high-luminosity end of the luminosity function is still poorly determined, with a variation in observed number abundance at fixed luminosity measured from different surveys at $z > 0.3$ being about a factor ~ 2 (Mullis et al. 2004).

6 DISCUSSION AND CONCLUSIONS

In this paper, we have revisited the observed X-ray scaling relationships between mass and temperature (M–T) and mass and luminosity (M–L), simultaneously with the temperature and luminosity functions. We have attempted to compare the observable quantities as directly as possible (i.e. without bolometric or cooling-flow corrections) with a simple suite of models in which a fiducial gas entropy distribution is shifted by a value $0.5 < K_{\odot}/K_{100} < 7$. In particular,

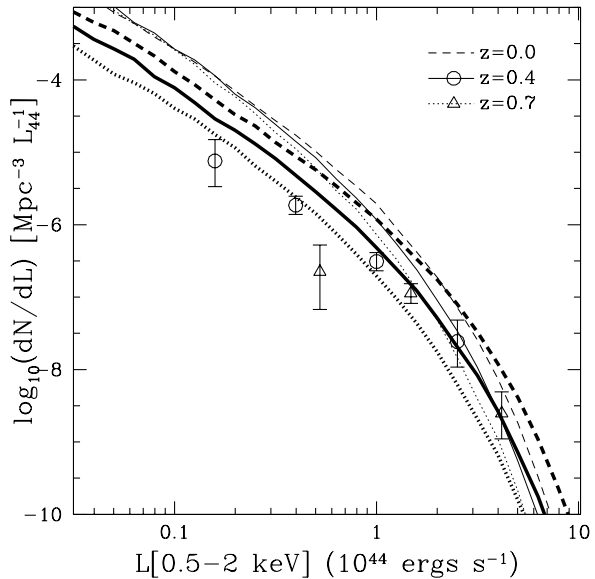


Figure 12. The luminosity functions at $z = 0, 0.4$ and $z = 0.7$, for the fixed-entropy ($2K_{100}$) models (thick lines) and the K_{cool} models (thin lines). Data at $z = 0.4$ and 0.7 are shown, from the WARPS survey, updated with *XMM-Newton* and *Chandra* luminosities for clusters at $z > 0.6$.

we focus on the scatter in the observed scaling relations, and how this compares with the scatter expected due to a) a range of halo structures (concentrations); b) the time available for cooling-only processes or c) heating/cooling efficiency. Since cluster temperatures are relatively insensitive to variations in the entropy distribution (and hence the scatter in the M–T relation is small), we gain the most by focusing on the M–L relation and the luminosity function. Our main findings are as follows:

(i) The variations in dark matter halo concentration expected from simulations are not large enough to account for the scatter in the observed M–L relation of clusters and groups.

(ii) Simple models of the intracluster medium in which the core entropy is modified to have a minimum value require the value of this floor to be between about $0.5K_{100}$ and $7K_{100}$ to match the slope, normalization and scatter in the observed M–T and M–L scaling relations. The constraint comes mostly from the M–L relation, as the temperature is insensitive to the value of K_{\odot} .

(iii) The shape of the luminosity function is sensitive to the scatter in the M–L relation. The observations lie between the models with $K_{\odot} = 0.5K_{100}$ and $K_{\odot} = 7K_{100}$, but closer to the higher-entropy model. The scatter in entropy levels as a function of halo mass must be accounted for if the parameters σ_8 or K_{\odot} are to be accurately deduced from the luminosity function alone.

(iv) The model temperatures are in good agreement with the observed temperature function, assuming the mass function of Evrard et al. (2002). However, the insensitivity of temperature to K_{\odot} , and the uncertainty on the normalization parameter σ_8 , means this does not put strong constraints on the value (or range of values) of K_{\odot} .

(v) The amount of gas that can cool in a Hubble time sets

a maximum value on the minimum entropy of intracluster gas, K_o . Lower entropy floors can be achieved by allowing some gas to cool below the threshold, or reducing the time available for cooling. However, although this model provides a reasonable match to the median mass-luminosity relation, it cannot account for the many clusters with luminosities below this relation.

(vi) We also present predictions for the evolution of the scaling relations and temperature/luminosity functions, out to $z = 0.7$. A comparison with observations suggests that the model with $K_o = 2K_{100}$ is valid out to $z \sim 0.7$, but this depends on how the scatter in the M-L relation evolves, which is currently unknown. On group scales, where observations unfortunately will be most difficult, these predictions clearly distinguish between an entropy floor K_o that is independent of mass and redshift, and one that is tied to the cooling time of a halo.

Thus, the scatter in the observations can be understood if the minimum entropy of the gas in clusters has a median value of $K_o = 200$ keV cm 2 but varies by a factor ~ 3 between halos of similar mass. Although we lack a quantitative theoretical prediction for the origin of this scatter, it seems reasonable to associate it with a similar range in the efficiency of heating and/or cooling.

We acknowledge that the models presented here provide an incomplete description of the intracluster medium. Apart from the obvious point that the pure heating models neglect the cooling processes that must take place to form the galaxies and AGN responsible for the heating in the first place, these models also lead to isentropic core gas distributions that are in conflict with at least some high resolution observations of clusters (e.g., Ponman et al. 2003; Pratt & Arnaud 2005). Therefore, cooling must be incorporated for a full description of the data. Although we have made a very crude step in this direction by tying the entropy floor level to the cooling time available, this model is greatly oversimplified, as it does not allow the gas to flow to the centre as it cools as in more realistic models (e.g. VBBB). Furthermore, for low mass clusters and groups this model predicts too much condensed gas, as most of the intracluster medium in a self-similar model has an entropy below the cooling threshold. Therefore, some combination of heating and cooling is expected to be required.

Such a model has recently been developed by McCarthy et al. (2004); in this model, preheated gas is allowed to cool in a realistic way, following the hydrodynamic evolution of the gas as it flows to the centre. With an appropriate range of preheating levels and cooling times, this model can reproduce the slope, normalization and the scatter in the M-L relation. Our results show that including scatter in the halo potentials (not considered by McCarthy et al.) would only have a secondary impact on their constraints. We have also explored the effect of scatter on the temperature and luminosity functions. Since the M-T relation is relatively insensitive to the gas distribution (as long as the very lowest entropy gas is heated or removed), we can expect that the predictions for the temperature function using the model of McCarthy et al. would be very similar to the models presented here. However, the luminosity function, and the evolution in the scaling relations, will be sensitive to the mass and redshift dependence of the distribu-

tions of preheating levels and cooling times. The next step, therefore, is to physically link these distributions through a feedback model, and to compare the resulting luminosity function with the observations.

Finally, we note that while analyses of the M-L and M-T relations and the luminosity and temperature functions can teach us much, they are only probing the integrated properties of the intracluster medium. Some of the most powerful constraints on the role of non-gravitational physics in mediating the properties of the ICM are likely to come from detailed comparisons of theoretical models to the actual spatially-resolved profiles (e.g., entropy and temperature) of clusters. The difficulty is in obtaining such profiles for large, representative samples of clusters and (especially) groups. However, as more and more groups and clusters observed with *Chandra* and *XMM-Newton* become publicly available, progress is beginning to be made on this front (e.g., Pratt & Arnaud 2005; Piffaretti et al. 2005; Cypriano et al. 2005). Such comparisons will make excellent complementary probes to studies such as the present one that make use of more easily obtained and robust integrated cluster properties.

ACKNOWLEDGEMENTS

We thank D. Horner for providing his cluster catalogues in electronic form, and we acknowledge useful discussions with Scott Kay and Paul Bode. MLB is grateful for the hospitality at University of Victoria, where this work was initiated, and acknowledges financial support from a PPARC fellowship PPA/P/S/2001/00298 and an NSERC Discovery grant. Research support for AB comes from the Natural Sciences and Engineering Research Council (Canada) through the Discovery grant program. AB would also like to acknowledge support from the Leverhulme Trust (UK) in the form of the Leverhulme Visiting Professorship at the Universities of Oxford and Durham. IGM acknowledges support from an NSERC postgraduate scholarship.

REFERENCES

- Arnaud M., Pointecouteau E., Pratt G. W., 2005, A&A, 441, 893
- Böhringer H., et al., 2001, A&A, 369, 826
- Babul A., Balogh M. L., Lewis G. F., Poole G. B., 2002, MNRAS, 330, 329 (BBLP)
- Balogh M. L., Babul A., Patton D. R., 1999, MNRAS, 307, 463
- Borgani S., Finoguenov A., Kay S. T., Ponman T. J., Springel V., Tozzi P., Voit G. M., 2005, MNRAS, 361, 233
- Borgani S., Governato F., Wadsley J., Menci N., Tozzi P., Quinn T., Stadel J., Lake G., 2002, MNRAS, 336, 409
- Bullock J. S., Kolatt T. S., Sigad Y., Somerville R. S., Kravtsov A. V., Klypin A. A., Primack J. R., Dekel A., 2001, MNRAS, 321, 559
- Burles S., Nollett K. M., Turner M. S., 2001, ApJL, 552, L1
- Cypriano E. S., Lima Neto G. B., Sodré L., Kneib J.-P., Campusano L. E., 2005, ApJ, 630, 38

- De Grandi S., Molendi S., 2002, *ApJ*, 567, 163
- Dolag K., Bartelmann M., Perrotta F., Baccigalupi C., Moscardini L., Meneghetti M., Tormen G., 2004, *A&A*, 416, 853
- Edge A. C., Stewart G. C., 1991, *MNRAS*, 252, 414
- Eke V. R., Cole S., Frenk C. S., 1996, *MNRAS*, 282, 263
- Eke V. R., Navarro J. F., Frenk C. S., 1998, *ApJ*, 503, 569
- Eke V. R., Navarro J. F., Steinmetz M., 2001, *ApJ*, 554, 114
- Ettori S., et al., 2004a, *MNRAS*, 354, 111
- Ettori S., et al., 2004b, *A&A*, 417, 13
- Evrard A. E., MacFarland T. J., Couchman H. M. P., Colberg J. M., Yoshida N., White S. D. M., Jenkins A., Frenk C. S., Pearce F. R., Peacock J. A., Thomas P. A., 2002, *ApJ*, 573, 7
- Fabian A. C., Crawford C. S., Edge A. C., Mushotzky R. F., 1994, *MNRAS*, 267, 779
- Hayashi E., Navarro J. F., Power C., Jenkins A., Frenk C. S., White S. D. M., Springel V., Stadel J., Quinn T. R., 2004, *MNRAS*, 355, 794
- Henry J. P., 2000, *ApJ*, 534, 565
- Henry J. P., 2004, *ApJ*, 609, 603
- Horner D., 2001, PhD thesis, University of Maryland
- Horner D. J., Mushotzky R. F., Scharf C. A., 1999, *ApJ*, 520, 78
- Ikebe Y., Reiprich T. H., Böhringer H., Tanaka Y., Kitayama T., 2002, *A&A*, 383, 773
- Jenkins A., Frenk C. S., White S. D. M., Colberg J. M., Cole S., Evrard A. E., Couchman H. M. P., Yoshida N., 2001, *MNRAS*, 321, 372
- Jing Y. P., 2000, *ApJ*, 535, 30
- Jones L. R., Ebeling H., Scharf C., Perlman E., Horner D., Fairley B., Wegner G., Malkan M., 2001, in *ASP Conf. Ser. 232: The New Era of Wide Field Astronomy The X-ray Evolution of Clusters of Galaxies to $z = 0.9$* . p. 141
- Kaiser N., 1991, *ApJ*, 383, 104
- Kauffmann G., White S. D. M., 1993, *MNRAS*, 261, 921
- Kay S. T., Thomas P. A., Jenkins A., Pearce F. R., 2004, *MNRAS*, 355, 1091
- Kotov O., Vikhlinin A., 2005, *ApJ*, 633, 781
- Lacey C., Cole S., 1994, *MNRAS*, 271, 676
- Lewis G. F., Babul A., Katz N., Quinn T., Hernquist L., Weinberg D. H., 2000, *ApJ*, 536, 623
- Loken C., Norman M. L., Nelson E., Burns J., Bryan G. L., Motl P., 2002, *ApJ*, 579, 571
- Lumb D. H., et al., 2004, *A&A*, 420, 853
- Markevitch M., 1998, *ApJ*, 504, 27
- Mathiesen B. F., Evrard A. E., 2001, *ApJ*, 546, 100
- Maughan B. J., Jones L. R., Ebeling H., Scharf C., 2006, *MNRAS*, 365, 509
- McCarthy I., Fardal M., Babul A., 2005, *ApJ*, submitted, *astro-ph/0501137*
- McCarthy I. G., Balogh M. L., Babul A., Poole G. B., Horner D. J., 2004, *ApJ*, 613, 811
- McCarthy I. G., Holder G. P., Babul A., Balogh M. L., 2003, *ApJ*, 591, 526
- Moore B., Governato F., Quinn T., Stadel J., Lake G., 1998, *ApJL*, 499, L5
- Muanwong O., Thomas P. A., Kay S. T., Pearce F. R., Couchman H. M. P., 2001, *ApJL*, 552, L27
- Mullis C. R., Vikhlinin A., Henry J. P., Forman W., Gioia I. M., Hornstrup A., Jones C., McNamara B. R., Quintana H., 2004, *ApJ*, 607, 175
- Navarro J. F., Frenk C. S., White S. D. M., 1996, *ApJ*, 462, 563
- Nevalainen J., Markevitch M., Forman W., 2000, *ApJ*, 536, 73
- Osmond J. P. F., Ponman T. J., 2004, *MNRAS*, 350, 1511
- Ostriker J. P., Bode P., Babul A., 2005, *ApJ*, 634, 964
- Piffaretti R., Jetzer P., Kaastra J. S., Tamura T., 2005, *A&A*, 433, 101
- Ponman T. J., Cannon D. B., Navarro J. F., 1999, *Nature*, 397, 135
- Ponman T. J., Sanderson A. J. R., Finoguenov A., 2003, *MNRAS*, 343, 331
- Power C., 2003, PhD thesis, University of Durham
- Pratt G. W., Arnaud M., 2005, *A&A*, 429, 791
- Randall S. W., Sarazin C. L., Ricker P. M., 2002, *ApJ*, 577, 579
- Rasia E., Mazzotta P., Borgani S., Moscardini L., Dolag K., Tormen G., Diaferio A., Murante G., 2005, *ApJL*, 618, L1
- Raymond J. C., Cox D. P., Smith B. W., 1976, *ApJ*, 204, 290
- Reiprich T. H., Böhringer H., 2002, *ApJ*, 567, 716
- Ritchie B. W., Thomas P. A., 2002, *MNRAS*, 329, 675
- Rowley D. R., Thomas P. A., Kay S. T., 2004, *MNRAS*, 352, 508
- Scharf C. A., Jones L. R., Ebeling H., Perlman E., Malkan M., Wegner G., 1997, *ApJ*, 477, 79
- Smith G. P., Kneib J., Smail I., Mazzotta P., Ebeling H., Czoske O., 2005, *MNRAS*, 359, 417
- Spergel D. N., Verde L., Peiris H. V., Komatsu E., Nolta M. R., et al., 2003, *ApJS*, 148, 175
- Tegmark M., Strauss M. A., Blanton M., et al., 2004, *Phys. Rev. D*, 69, 103501
- Thomas P. A., Muanwong O., Kay S. T., Liddle A. R., 2002, *MNRAS*, 330, L48
- Tozzi P., Norman C., 2001, *ApJ*, 546, 63
- Viana P. T. P., Kay S. T., Liddle A. R., Muanwong O., Thomas P. A., 2003, *MNRAS*, 346, 319
- Vikhlinin A., 2005, *ApJ*, submitted, *astro-ph/0504098*
- Vikhlinin A., Markevitch M., Murray S. S., Jones C., Forman W., Van Spekbroeck L., 2005, *ApJ*, 628, 655
- Vikhlinin A., VanSpekbroeck L., Markevitch M., Forman W. R., Grego L., 2002, *ApJL*, 578, L107
- Voit G. M., Balogh M. L., Bower R. G., Lacey C. G., Bryan G. L., 2003, *ApJ*, 593, 272
- Voit G. M., Bryan G. L., 2001, *Nature*, 414, 425
- Voit G. M., Bryan G. L., Balogh M. L., Bower R. G., 2002, *ApJ*, 576, 601 (VBBB)
- Wechsler R. H., Bullock J. S., Primack J. R., Kravtsov A. V., Dekel A., 2002, *ApJ*, 568, 52
- Williams L. L. R., Babul A., Dalcanton J. J., 2004, *ApJ*, 604, 18
- Zhao D. H., Mo H. J., Jing Y. P., Börner G., 2003, *MNRAS*, 339, 12